Earth and Planetary Science Letters 300 (2010) 1–10

Contents lists available at ScienceDirect

Earth and Planetary Science Letters

journal homepage: www.elsevier.com/locate/epsl

Steady-state laboratory flow laws alone fail to explain postseismic observations

Andrew M. Freed [a,*], Thomas Herring [b], Roland Bürgmann [c]

[a] Department of Earth and Atmospheric Sciences, Purdue University, West Lafayette, IN, USA
[b] Department of Earth, Atmospheric, and Planetary Sciences, Massachusetts Institute of Technology, Cambridge, MA, USA
[c] Department of Earth and Planetary Science, University of California Berkeley, Berkeley, CA, USA

ARTICLE INFO

Article history:
Accepted 5 October 2010
Available online 23 October 2010

Keywords:
postseismic relaxation
rheology
Hector Mine
dislocation creep
geodesy
finite element modeling

ABSTRACT

We test whether laboratory derived steady-state flow laws for wet olivine can be used to explain postseismic relaxation in the upper mantle following the 1999 Hector Mine earthquake. This is accomplished using rate changes in GPS observed displacement time-series at far-field stations as constraints on the parameters associated with laboratory derived temperature- and stress-dependent flow laws for diffusion and dislocation creep of olivine. We primarily concentrate on the influences of temperature, grain size, and background strain rate to explain observed fast early displacement rates that slow rapidly in the 7 years of postseismic observations. We find that a reasonable fit to the observed time-series cannot be achieved by any combination of flow law parameters and plausible assumptions for the tectonic environment of the mantle beneath the Mojave Desert. We conclude that postseismic relaxation within the mantle following the Hector Mine earthquake likely includes an initial transient weakening phase, suggesting that steady-state flow laws by themselves are insufficient to characterize the flow of mantle rocks when stress conditions evolve.

1. Introduction

Decades of laboratory rock squeezing experiments have been designed to determine how rocks below the seismogenic zone flow in response to differential stress. These experiments have lead to the recognition of a number of creep mechanisms and associated constitutive relationships that quantify how viscosity and flow strain rates vary as a function of mineralogy and tectonic environment (e.g., pressure, temperature, stress, and water content) (e.g., Carter and Tsenn, 1987; Kirby and Kronenberg, 1987). If grain sizes and differential stresses are relatively large, laboratory experiments suggest that flow should be dominated by dislocation creep (Hirth et al., 2001; Karato, 1997), which can be described by a steady-state temperature- and stress-dependent power-law of the form,

$$\dot{\varepsilon} = AC_{\mathrm{OH}}^{r}\sigma^{n}e^{-(Q+PV^{*})/RT}, \tag{1}$$

where ($\dot{\varepsilon}$) is the strain rate, A is a pre-exponential factor ($\mathrm{MPa}^{-n}\mathrm{s}^{-1}$), C_{OH} is water content (molar hydroxyl concentration, ppm H/10^6Si), r is the water content exponent, σ is the differential stress (MPa), n is the stress exponent, Q is the activation energy (kJ/mol), P is pressure (Pa), V^* is activation volume (cm^3/mol), R is the universal gas constant ($\mathrm{J\,mol}^{-1}\,\mathrm{K}^{-1}$), and T is temperature (K) (e.g., Hirth and Kohlstedt, 2003).

If grain sizes and differential stresses are relatively small, laboratory experiments suggest that steady-state flow should be dominated by diffusion creep (Karato, 1997), which can be described by

$$\dot{\varepsilon} = AC_{\mathrm{OH}}^{r}d^{-p}\sigma e^{-(Q+PV^{*})/RT}, \tag{2}$$

where d is the grain size (μm), and p is the grain size exponent. The major difference between these two mechanisms is the power-law dependence of dislocation creep on stress, and the dependence of diffusion creep on grain size.

As both the grain size and stress state of the uppermost mantle are uncertain and potentially within the range of the transition between these creep mechanisms (order 1 mm for grain size and 0.1–1 MPa for stress, Karato, 1997), it is unclear which flow law likely characterizes mantle rheology at these depths — and this could vary amongst tectonic environments. Furthermore, laboratory experiments generally require large extrapolations to go from experimental stress and strain rates to tectonic ones, raising some uncertainty with regards to their appropriateness to describe *in situ* behavior.

It is also not clear if steady-state flow laws are sufficient to describe the complete response of a viscous mantle to a change in the stress environment. Several laboratory experiments suggest that in response to a change in loading conditions, an initial transient phase marked by more rapid flow strain rates precedes a slower steady-state response (e.g., Carter and Kirby, 1978; Chopra, 1997). Pollitz (2003, 2005) argued that inclusion of an initial transient weakening phase was required to explain observed surface displacement rate changes following the 1999 Hector Mine, California and 2002 Denali, Alaska earthquakes. In such

* Corresponding author. Tel.: +1 765 496 3738; fax: +1 765 496 1210.
E-mail address: freed@purdue.edu (A.M. Freed).

0012-821X/$ – see front matter
doi:10.1016/j.epsl.2010.10.005

postseismic deformation studies, large earthquakes are used as *in situ* rock squeezing experiments, where a sudden increase in differential stress in the lower crust and upper mantle induced viscous flow. This flow causes a transfer of stress back to the upper crust, inducing geodetically observable postseismic surface deformations that can then be used to constrain numerical models of this relaxation process (see review by Bürgmann and Dresen, 2008). In the postseismic studies conducted by Pollitz (2003, 2005), fast early postseismic displacement rates that slowed dramatically were explained by a mantle with an initial transient viscosity an order of magnitude lower than that inferred for eventual steady-state flow.

These previous postseismic studies did not, however, take into account the stress-dependence of steady-state power-law flow. The viscosity (η) of a power-law rheology can be expressed as,

$$\eta = \sigma^{1-n} e^{(Q + PV^*)/RT} / 2AC_{OH}^{r}. \quad (3)$$

With a typical value of $n = 3$–4 for mantle rocks (e.g., Carter and Tsenn, 1987; Kirby and Kronenberg, 1987), this implies that viscosity is inversely proportional to stress raised to a power of 2–3. Thus, coseismic stress increases caused by an earthquake would act to temporarily reduce viscosity, with viscosity recovering to background levels as coseismic stresses are dissipated. Freed and Bürgmann (2004) and Freed et al. (2006) used the stress-dependence of dislocation creep associated with wet olivine to explain the non-linear response of the Landers, Hector Mine, and Denali earthquakes. However, while these power-law analyses were able to explain postseismic relaxation rates, the number and duration of GPS displacement time-series constraints were limited. Each analysis utilized 6 or less far-field stations — those far enough away from the fault (~1 rupture length) to not be substantially influenced by near field processes (poroelastic flow, afterslip, and lower crustal flow). Moreover, each analysis utilized time-series durations of no more than 3 years, which only covers a small portion of the full relaxation time period (at least a decade). Thus it remains uncertain as to whether stress-dependent power-law steady-state flow is sufficient to explain observed postseismic displacement rate changes, or whether an initial transient weakening phase must be active.

Here we test the hypothesis that a steady-state, stress-dependent power-law rheology alone is sufficient to explain postseismic displacement time-series following the 1999 Hector Mine earthquake using 7-year-long time-series at 55 far-field GPS stations (Fig. 1). Seven years of post-Hector Mine observations reveal displacements of sites more than several fault lengths from the rupture surface that could only be due to mantle flow below ~40 km depth (Freed et al., 2007). A sampling of the time-series is shown in Figure 2, which are functional representations of the time-series data for different assumption of logarithmic decay time (discussed below). The objective is to determine if any combination of reasonable power-law and environmental parameters for the mantle beneath the Eastern California Shear Zone (ECSZ), the tectonic province in which the earthquake occurred, can be used to explain the observed time-series. If so, this would suggest that a transient phase may not significantly participate in the postseismic response of the mantle. If a plausible set of parameters cannot be found, it would imply that a transient phase may be a ubiquitous process in the response of the mantle to a sudden change in the regional stress field. For completeness, we also test the hypothesis that steady-state diffusion creep of olivine can explain far-field post-Hector Mine surface displacements.

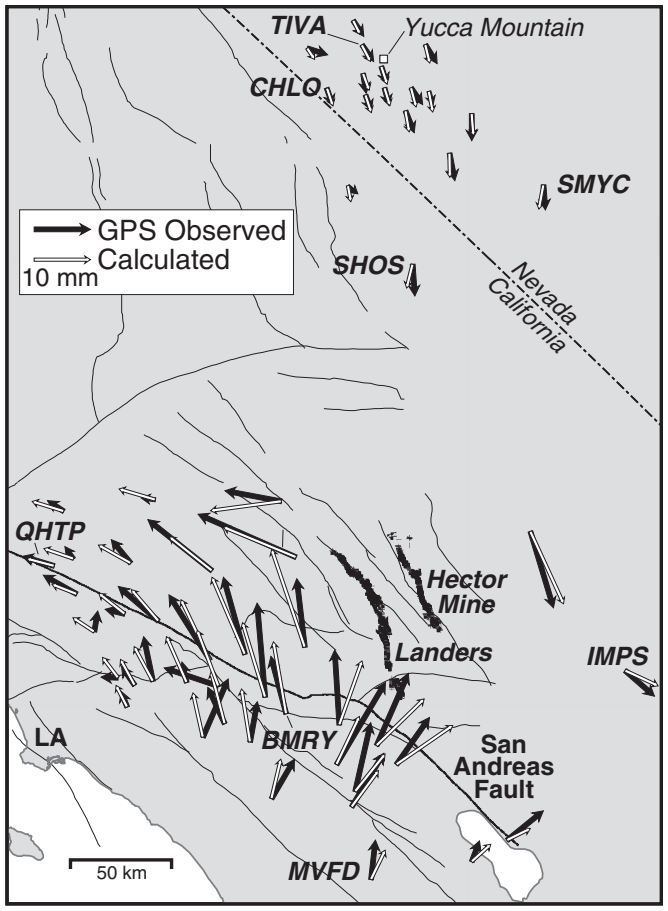

Fig. 1. Cumulative GPS observed postseismic horizontal surface displacements (transient component) for the 7 year period following the 1999 Hector Mine earthquake compared to those calculated by the best-fitting model of steady-state dislocation creep of a wet olivine upper mantle. Stations within about one rupture length of the Hector Mine rupture surface have been excluded limit comparisons to stations where surface displacements are primarily due to mantle flow.

2. GPS displacement time-series

Daily time-series following the Hector Mine earthquake are obtained from continuously operating GPS sites, most of which are part of the SCIGN network that became operational between 1996 and 2001. The time-series are used to estimate linear interseismic displacement rates, coseismic offsets, and a logarithmically and/or exponentially decaying function that represents the postseismic signal. Postseismic components include viscoelastic relaxation following the 1999 M7.1 Hector Mine earthquake, as well as continued deformation from the nearby 1992 M7.3 Landers earthquake (Fig. 1). The analysis of the GPS data was carried out in two phases. In the first phase, we determined the positions and velocities of a group of 40 sites that define our stable North America reference frame. The MIT weekly solution independent exchange (SINEX) format files, processed using absolutes phase center models for both ground and satellite antennas, and available from the crustal dynamics data information center (CDDIS) (ftp://cddis.gsfc.nasa.gov/gps/products/wwww/repro1 where wwww is the GPS week numbers) were used in this analysis. Data from GPS weeks 0843 (Jan 1996) to 1514 (Jan 2009) were included. Care was taken in selecting reference frame sites for this analysis so that no site within 400 km of the Hector Mine epicenter was included. We allowed for possible position offsets in the stations when antennas and/or radomes were changed. For this study, the North America plate was defined using the North America Euler pole given in the ITRF2005 reference frame (Altamini et al., 2007). In Supplementary Figure S1, we show a map of the sites used to define the reference frame for the Hector Mine pre- and postseismic motion analysis. The results are tabulated in Supplementary Table S1. Data collected between Jan 1, 1996 and Jan 18, 2009 were used to define the motion of sites used for establishing the reference frame and in the analysis of Hector Mine accumulated postseismic motion. The

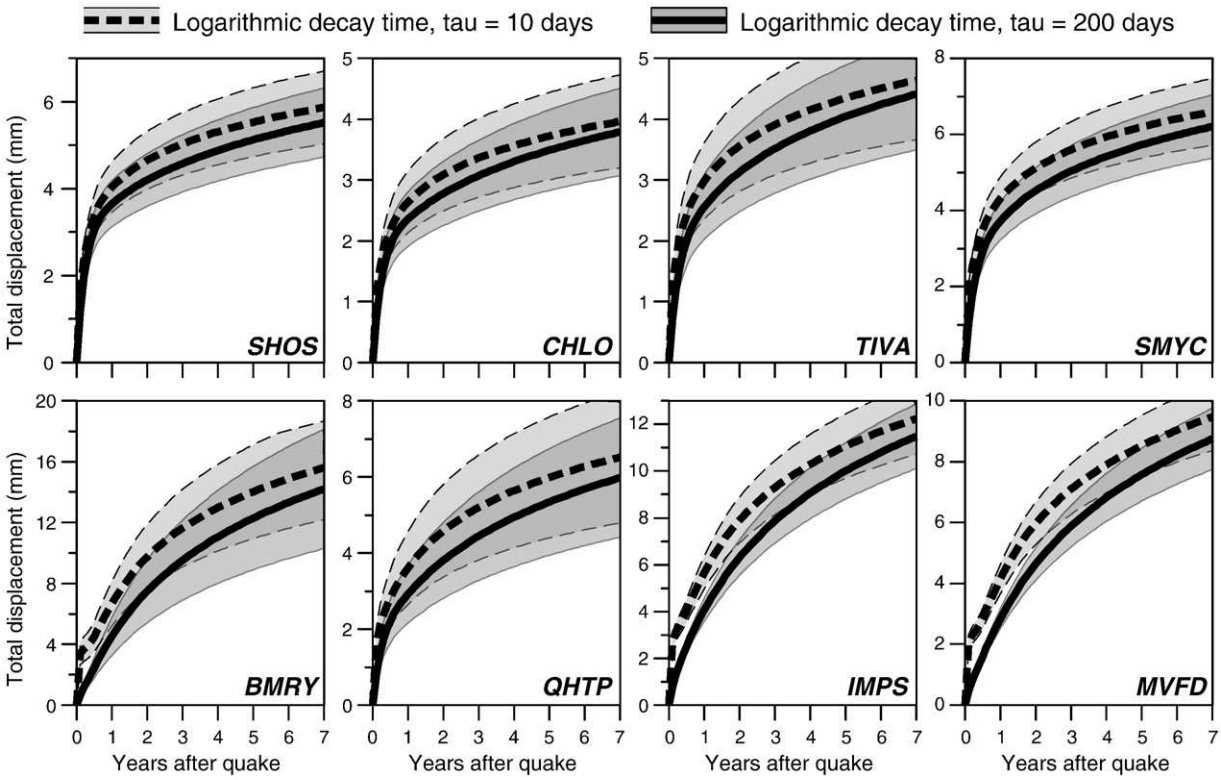

Fig. 2. Functional representations of displacement time-series for a number of far-field stations (labeled in Fig. 1) for two logarithmic decay times: a very short decay time of $\tau = 10$ days and a relatively long decay time of $\tau = 200$ days. Both representations assume an exponential decay time of 80 days. 1σ error bars shown in grey.

alignment of the GPS solution to the ITRF2005 system, as realized by the IGS05 coordinates and velocities (Ferland, 2006), was achieved through rotation and translation offsets and rates. No scale or scale rates were included in the alignment.

With the positions and velocities of the 40 reference frame sites determined, we transformed the raw Cartesian coordinate time-series files, processed with absolute phase center models, generated by the Scripps Institution of Oceanography and available at http://garner.ucsd.edu/pub/timeseries (specifically we used rawXyzTimeSeries20090123.tar) into this frame by estimating daily rotations and translations to be applied to the time-series. To the transformed time-series, we fit models consisting of a linear trend, offsets at times of antenna and/or radome changes and earthquakes, annual periodic signals, and one of four parameterizations for postseismic deformation after the Hector Mine earthquake. The four parameterizations are a combination of logarithmic variation of the form,

$$dp_l = A_l \log\left(1 + \left(t - t_{eq}\right)/\tau_l\right) \quad t > t_{eq} \tag{4}$$

and an exponential decay of the form,

$$dp_e(t) = A_e\left(1 - e^{\left(t-t_{eq}\right)/\tau_e}\right) \quad t > t_{eq} \tag{5}$$

where $dp_l(t)$ and $dp_e(t)$ are the position changes in the north, east, or height directions as a function of time, t. The amplitudes of the signals A_l and A_e were estimated simultaneously with the other parameters. The time constants τ_l and τ_e were held fixed at constant values. We considered four parameter sets: (1) $\tau_l = 10$ days, no exponential term; (2) $\tau_l = 10$ days, and $\tau_e = 80$ days; (3) $\tau_l = 200$ days, no exponential term; and (4) $\tau_l = 200$ days, and $\tau_e = 80$ days. From the estimated log and exponential coefficients, we estimated the total displacement after 7 years, and the uncertainty of the total displacement using a correlated noise model and the variance–covariance matrix of the log and exponential coefficients when both were estimated.

The correlated noise model characterizes the time-series noise as a combination of white noise and a first-order-Gauss Markov process where the variances and time constants of the noise processes were estimated from the residuals to the time-series fit. The estimated total displacements with 95% confidence interval error ellipses, for sites where the standard deviation of the horizontal motion estimates were less than 2 mm, are shown in Supplementary Figures S2a, S2b, and S2c. For most far-field sites (those located more than about one rupture length form the rupture surface), the total displacement results do not depend critically on the parameterization chosen. The near field sites are affected by the choice and for these sites a combination of both logarithmic and exponential decays are needed to model the time-series. The estimated displacements from the 200-day log and 80-exponential model are given in Supplementary Table S2 for the horizontal displacements for all sites with standard deviations less than 3 mm. The minimum and maximum values for the east and north displacements from these analyses are also provided in the table. Supplementary Table S3 shows the corresponding accumulated motions in heights.

Examples of the functional representation of time-series data used in the analysis are shown in Supplementary Figure S3. The daily determinations of the north positions, after removing the estimated linear trend and non-earthquake offsets, are shown for a selection of sites along an approximately north–south profile through the Hector Mine rupture. The Hector Mine coseismic offset, postseismic motion and annual signals are retained in the residuals shown. Superimposed on the daily determinations are annual averages and the model parameter estimates of the coseismic offset, postseismic motion (combination of 200-day log and 80-day exponential) and annual periodic terms. The root-mean-square RMS differences of the annual averages from the model fit range between 0.06 and 0.25 mm.

Functional representations of displacement time-series are moderately influenced by the parameterization, in particular the assumed

logarithmic decay time. Figure 2 shows examples of functional representations for a number of far-field stations (labeled in Fig. 1) for two logarithmic decay times, a very short decay time of $\tau = 10$ days and a relatively long decay time of $\tau = 200$ days. The 10 day decay time representation leads to faster initial displacement rates compared to the 200 day decay time representation, especially for the sites closer toward the rupture. We use the 200 day decay time representation for the test of rheological models, as it provides the minimum rate changes that a model needs to match to be considered plausible. If a candidate rheology cannot match these initial displacement rates, it will not be able to match any that consider shorter decay times.

3. Modeling approach

To test whether steady-state flow laws are sufficient to explain post-Hector Mine time-series, we use a finite element model of the southwestern US centered at the epicenter of the Hector Mine earthquake similar to that utilized in our previous Newtonian rheology study (Freed et al., 2007). The model extends 700 km in all directions from the Hector Mine epicenter and to a depth of 400 km, sufficient distance such that fixing these boundary conditions does not influence results as they are far beyond the reach of coseismic stress changes. This model simulates coseismic slip associated with both the 1992 M7.3 Landers (Fialko, 2004) and 1999 M7.1 Hector Mine (Simons et al., 2002) earthquakes (verification of the coseismic models was discussed in Freed et al. (2007)). As these earthquakes occurred in relatively close proximity (25 km distance) and post-seismic relaxation from the Landers event is ongoing following the Hector Mine event, both earthquakes were considered in the simulation. For the present study we have added velocity boundary conditions that generate a regional strain rate field across the ECSZ region. For each candidate power-law rheology, we apply these velocity boundary conditions until steady-state stress levels are achieved in the lower crust and upper mantle. Since the differential stress in Eq. (1) is the total differential stress (background plus coseismic), the background stress level is a very important factor in how the mantle rocks will respond to coseismic stress changes. Since it does not relax, the background stress state of the upper crust does not influence calculated postseismic displacements. Once steady-state is achieved, the Landers coseismic slip is initiated, the crust and mantle are allowed to relax for 7 years of model time, then the Hector Mine rupture is imposed and another 7 years of relaxation take place. It is this latter 7-year period for which surface displacements at the GPS station locations are calculated for comparison to observed postseismic time-series.

The parameters that control the calculated response of a visco-elastic upper mantle to sudden coseismic stress changes can be divided into two categories, flow law parameters (A, r, p, n, Q, and V in Eqs. (1) and (2)) and environmental parameters (d, C_{OH}, σ, and T). The uncertainties in these parameters track into uncertainties in effective viscosity and resulting surface displacement rates. Having deduced that far-field surface displacements are associated with flow in the mantle (Freed et al., 2007), we assume that this flow is associated with the creep of olivine, which is believed to govern the rheology of Earth's upper mantle as it is the most abundant phase (with a volume fraction of ~60%) and also the weakest in most cases (e.g., Borch and Green, 1987; Handy, 1990; Karato and Wu, 1993). We test laboratory flow law parameters for the creep of olivine using parameters as suggested by Korenaga and Karato (2008), based on a statistical analysis of a number of rock deformation experiments (Hirth and Kohlstedt, 1995; Jung et al., 2006; Karato, 1986; and Mei and Kohlstedt, 2000a,b), and on flow law parameters as suggested by Hirth and Kohlstedt (2003). Table 1 shows the flow law parameter sets considered in this analysis, including upper and lower end-member strength (high viscosity/low viscosity) models for Korenaga and Karato wet rheologies. Hirth and Kohlstedt (2003) did not report the uncertainties associated with the pre-exponential factor, making it difficult to quantify uncertainties in viscosity from these parameters.

To provide an idea of how these flow law parameter sets relate to viscosity, the last column in Table 1 shows the resulting viscosity for an example mantle environment that might be found at a depth of 50 km in a recent backarc setting such as that of southern California ($T = 1000$ °C, $C_{OH} = 800$ ppm H/10^6Si, $d = 1$ mm, and $\sigma = 0.3$ MPa). For the wet dislocation models, uncertainties in flow law parameters lead to an uncertainty in viscosity of about an order of magnitude for this particular tectonic environment. The dry rheology model leads to a significant increase (3–5 orders of magnitude) in viscosity at these conditions, almost solely due to the removal of the water weakening term for dry rheologies. This extra strength can be compensated for if the temperature at this depth is ~300 °C hotter than the hottest

Table 1
Flow law parameters used in this study. K&K, 2008: Korenaga and Karato (2008), and H&K, 2003: Hirth and Kohlstedt (2003). Viscosities (last column) are based on a tectonic environment of a depth of 50 km, average density of overburden of 3000 kg/m^3, $T = 1000$ °C, $d = 1$ mm, $s = 0.3$ MPa, and $C_{OH} = 800$ ppm H/10^6Si for wet rheologies and 0 ppm for dry rheologies. Note that these values do not correspond to the ranges of A shown in their Table 3, which does not take into account the covariance between A and the other parameters, particularly Q.

	A (MPa^{-n})	r	p	n	Q (kJ/mol)	V (cm^3/mol)	η (Pa s)
Wet dislocation							
K&K, 2008, low η	$10^{-3.57}$[a]	2.00	n/a	3.84	423	1	2.34×10^{22}
K&K, 2008, median η	$10^{0.6}$	1.95	n/a	3.60	523	4	3.19×10^{22}
K&K, 2008, high η	$10^{4.66}$[a]	1.90	n/a	3.36	623	7	5.59×10^{22}
H&K, 2003	$10^{1.95}$	1.20	n/a	3.50	480	11	8.80×10^{21}
Dry dislocation							
K&K, 2008, median η	$10^{6.09}$	n/a	n/a	4.94	610	13	3.15×10^{27}
H&K, 2003	$10^{5.04}$	n/a	n/a	3.50	530	20	3.83×10^{25}
Wet diffusion							
K&K, 2008, low η	$10^{2.57}$[a]	2.00	2.80	n/a	334	21	5.26×10^{20}
K&K, 2008, median η	$10^{4.32}$	1.93	2.56	n/a	387	25	7.48×10^{20}
K&K, 2008, high η	$10^{6.07}$[a]	1.86	2.32	n/a	440	29	1.10×10^{21}
H&K, 2003	$10^{6.0}$	1.00	3.0	n/a	335	4	6.13×10^{19}
Dry diffusion							
K&K, 2008, median η	$10^{5.25}$	n/a	2.98	n/a	261	6	2.93×10^{20}
H&K, 2003	$10^{9.17}$	n/a	3.0	n/a	375	6	1.92×10^{21}

[a] End-member values for A are based on Eqs. 20 and 22 of Korenaga and Karato (2008) using the end-member values for the respective creep parameters shown in their Table 2.

inferred geotherm, suggesting a dry dislocation creep rheology is unlikely.

Uncertainties in wet diffusion parameters lead to similar variations in viscosity for this particular environment. (Note that you cannot easily compare dislocation and diffusion creep viscosities as the former is influenced by choice of stress, while the latter is influenced by assumed grain size). In contrast to the dislocation case, the dry diffusion viscosity is comparable to the wet diffusion viscosity for these particular conditions. This is due to the trade-off between the weakening effects of water for the wet case and the much lower activation energy and volume associated with the dry case. These trade-offs make it difficult to distinguish between wet and dry diffusion rheologies, so we only consider the former as the upper mantle in former backarc settings is likely to have significant traces of water (e.g., Hirth and Kohlstedt, 1996).

Uncertainties in environmental parameters are generally not well constrained, but can be estimated based on a variety of geophysical observations. The thermal gradient in southern California has been inferred from variations of attenuation and shear velocities (see also Hyndman et al., 2009; Yang and Forsyth, 2008;). From this data, median and hot and cold end-member geotherms were constructed (Fig. 3a). The seismic data are not particularly sensitive to temperature below 100 km depth, and so converged on a similar geotherm at that depth. Thus, there is more uncertainty in the temperature estimates below 100 km than suggested by the figure. However, postseismic relaxation is not particularly sensitive to temperatures below 100 km, as significant coseismic stresses did not penetrate below this depth. The cold geotherm reaches a temperature of 900 °C at 50 km depth. Using the median flow law parameters for dislocation creep of wet olivine (Table 1), and the same example environmental parameters discussed earlier, this would lead to a viscosity of 2.26×10^{24} Pa s. The hot geotherm reaches a temperature of 1240 °C at 50 km depth, leading to a viscosity of 1.15×10^{19} Pa s, five orders of magnitude less. Thus, the uncertainty in temperature has a much greater influence on uncertainties in viscosity structure than that associated with uncertainties in laboratory derived flow law parameters. The laboratory parameter uncertainties correspond to about a 90 °C differences in temperature, compared to a 340 °C uncertainty in the temperature estimates in the region where postseismic relaxation following the Hector Mine earthquake is most vigorous. Thus, we only utilize the Korenaga and Karato (2008) median flow law parameter values in our analysis, ascribing most of the uncertainties to temperature and other environmental constraints. The results discussed below will show that it will take substantially more than the 90 °C difference that could be accounted for by uncertainties in flow law parameters to find a steady-state rheological model that satisfies observed post-Hector Mine time-series.

The water content of a mantle wedge (the mantle beneath the ECSZ is a former backarc region that may still hold the same water content as an active mantle wedge) has been inferred from infrared spectroscopic analysis on nominally anhydrous minerals in mantle xenoliths, which suggests that wedge olivine contains water at concentrations ranging from hundreds to thousands of H/10^6Si (Bell and Rossman, 1992). For the median wet dislocation flow law parameters and example environmental values discussed earlier, a range of water content varying from 500 to 2000 H/10^6Si leads to a range in calculated viscosity of 7.97×10^{22} to 5.32×10^{21} Pa s, about an order of magnitude variation. Though larger than the viscosity range associated with flow law parameter uncertainties, this range is much smaller than that associated with temperature uncertainties. Thus we will utilize a median value of 800 H/10^6Si (as suggested for the water content of continental asthenosphere by Hirth and Kohlstedt (1996) in all of our models.

The differential stress term in Eq. (1) represents the total differential stress, which includes long-term (steady-state) background stresses plus coseismic stress changes. Coseismic stress changes depend on the earthquake slip distribution and the elastic structure of the lithosphere, both of which are reasonably well constrained. But the magnitude of the background differential stress field within the mantle is perhaps the least constrained of all environmental parameters, as there are no means of directly measuring this quantity at depth. Where the mantle is weak enough to flow significantly in the years following an earthquake to induce measurable surface displacements, stresses may range from 0.1 to 1.0 MPa, though they could be higher or lower. For the median wet dislocation flow law parameters and example environmental values discussed earlier, such a variation in stress leads to a range in calculated viscosity of 5.54×10^{23} to 1.39×10^{21} Pa s, more than 2 orders of magnitude.

Though we cannot directly measure the background stress state, for steady-state flow it will be linearly proportional to the regional strain rate ($\sigma=2\varepsilon Y_r\eta$), which is at least measureable at the surface. The Hector Mine earthquake occurred in the ECSZ, which is characterized by a right-lateral strain rate (azimuth of N40°E) of the order of 0.1 μstrain/yr (Savage et al., 2003). While this interseismic strain rate is most likely uniform with depth through the relatively strong upper crust, it is unknown how this strain rate varies with

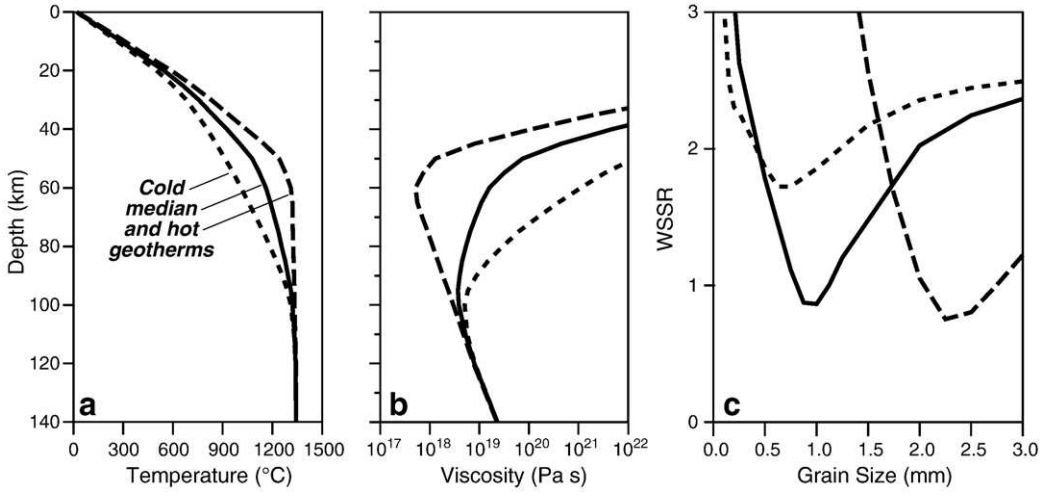

Fig. 3. (a) Seismically inferred range of thermal gradients beneath the Mojave Desert (Yang and Forsyth, 2008). (b) Calculated viscosity based on diffusion creep of wet olivine (median parameters, Table 1), a grain size of 1 mm, water content of 800 H/10^6Si, and the three thermal gradients shown in (a). (c) Misfit (WSSR) of calculated cumulative (7 years) postseismic surface displacements as a function of grain size and thermal gradient. We quantify WSSR as $sqrt[(1/m)\sum(d_o-d_c)^2/\sigma^2]$, where d_o and d_c are the observed and calculated displacements, σ is the observational error, and m is the total number of observations.

depth through the lower crust and mantle. In our modeling we vary the background stress within the mantle by varying the background strain rate through the application of velocity boundary conditions. Thus, instead of discussing the background stress directly, we parameterize this variable in terms of the background strain rate, which affords us the ability to discuss the modeled mantle strain rate relative to the strain rate observed at the surface (0.1 μstrain/yr).

For models that consider diffusion creep, we also must consider how the variation in grain size influences viscosity. The transition from dislocation to diffusion creep of olivine is dependent on both the background differential stress and grain size. For wet olivine at a differential stress of 1 MPa, the transition should occur at a grain size of ~1 mm, and for a differential stress of 0.1 MPa the transition should occur at ~3 mm (Hirth and Kohlstedt, 2003). While the grain size of olivine within the upper mantle beneath the Mojave Desert is not well constrained, it may be in the realm of 1–10 mm (Karato, personnel communication). Thus, depending on the background stress state, viscous flow within the upper mantle could be dominated by either diffusion or dislocation creep, or a combination. For the median flow law parameters for wet diffusion and the example environmental parameters discussed above, varying the grain size from 0.1 mm to 1.0 mm leads to a variation in viscosity from 2.06×10^{18} to 7.48×10^{20} Pa s, though the range of uncertainty could be larger.

Based on how uncertainties in flow law and environmental parameters track into uncertainties in viscosity from the above discussion, we limit our numerical experiment to consider median steady-state flow law parameters for olivine (Table 1), and variations in temperature, background strain rate (for dislocation creep models only), and grain size (for diffusion creep models only). We seek to determine what set of flow law parameters and tectonic conditions are required to explain both cumulative and time-series observations of surface displacements following the 1999 Hector Mine earthquake. For models that can satisfy these constraints, we then examine whether the numerically required tectonic environment is plausible in order to conclude whether post-Hector Mine surface displacements are likely a function of steady-state creep of olivine.

4. Results

We initially consider a suite of models in which we assume that postseismic relaxation following the Hector Mine earthquake is due to diffusion creep of wet olivine. Using median flow law parameters (Table 1) and a water content of 800 ppm H/10^6Si, we calculated postseismic displacements as a function of grain size and thermal gradient. Fig. 3b shows how viscosity of this model varies as a function of depth for each of the three thermal gradients shown in Figure 3a (with a grain size of 1 mm assumed). Note how the viscosity profile associated with the cold geotherm leads to the lowest viscosity occurring at a depth of ~100 km, while the viscosity profile associated with the hot geotherm leads to a minimum viscosity at a depth of only ~60 km. The depth of maximum postseismic flow is influenced by both the viscosity gradient and the stress gradient, but it is easy to see that the warmer the thermal gradient, the shallower the most rapid postseismic flow will tend to be.

Figure 3c shows the weighted sum of squared residuals (WSSR) for calculated cumulative (7 years) displacements for a suite of wet diffusion creep models as a function of grain size and thermal gradient. There is a trade-off between grain size and temperature for warmer thermal gradients (median and above), but a cooler geotherm leads to greater misfit. The best-fitting models fall in a range of grain size between 1.0 and 2.5 mm for thermal gradients that range from nominal to hot, respectively. Maximum postseismic flow in these models occurs in the range between about 45 and 70 km depth with viscosities of the order of 10^{19} Pa s. The best-fitting diffusion model

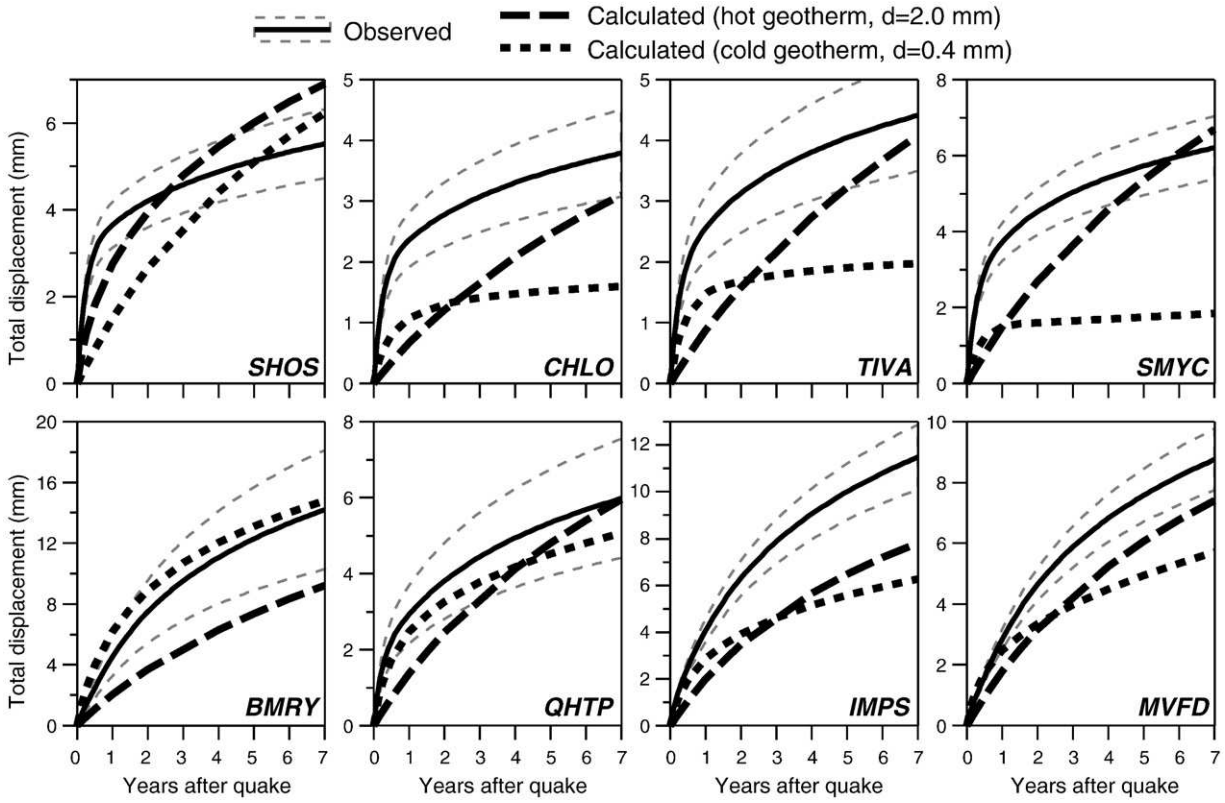

Fig. 4. Comparison between observed (functional representations) and calculated displacement time-series for a number of far-field stations (labeled in Fig. 1) for two models of diffusion creep. The observed time-series are based on a logarithmic decay time of $\tau=200$ days with 1σ error bars shown in thin dashed lines. The calculated models represent the best-fitting rheologies based on matching cumulative displacements (Fig. 3c) for assumed hot and cold geotherms (Fig. 3a).

associated with the cold geotherm cannot match cumulative displacements at many stations, particularly in the Yucca Mountain Region (stations CHLO, TIVA, and SMYC). This is because the cold geotherm leads to fairly deep (>80 km) postseismic flow, which leads to a poorly fitting deformation wavelength.

While wet diffusion creep models can be used to explain cumulative displacements, such models do not lead to rate changes in surface displacements consistent with GPS time-series. Figure 4 shows a comparison of calculated time-series from the best-fitting diffusion creep models for assumed hot and cold geotherms. Though the rheology associated with the hot geotherm provides a reasonable fit to 7 years of cumulative displacements, it invariably underpredicts displacement rate changes in the first couple of years following the earthquake, and overpredicts rates beyond a couple of years. No combinations of diffusion creep and environmental parameters could be found that lead to calculated surface displacements consistent with the observed surface displacement rate changes. This leads us to conclude that steady-state diffusion creep of wet olivine cannot by itself explain post-Hector Mine displacement time-series.

We next consider models that utilize flow law parameters associated with dislocation creep of wet olivine. For these models we use the median values for the flow law parameters (Table 1), vary the background strain rate (to vary the background stress state), and consider the seismically inferred range of possible thermal gradients (water content remains at 800 ppm H/10^6Si). By assuming a uniform-with-depth differential stress of 0.3 MPa, Figure 5a shows how the various thermal gradients influence the viscosity structure. As with the diffusion models, the colder the geotherm is, the deeper the postseismic flow.

Figure 5b shows the misfit of calculated cumulative (7 years) displacements for a suite of wet dislocation creep models as a function of background strain rate in the mantle and thermal gradient. As with the diffusion creep models, maximum postseismic flow in the best-fitting models occurs between about 45 and 70 km depth, with viscosities of the order of 10^{19} Pa s. There is a significant trade-off between background strain rate and temperature, with the best-fitting models for the hot, median, and cold geotherms requiring background strain rates of 0.16, 0.3, and 1.0 μstrain/yr, respectively, in order to fit 7-year cumulative displacements. These models all require a greater background strain rate than the 0.1 μstrain/yr observed (Savage et al., 2003). While it is relatively easy to explain why background strain rates might decrease with depth as weaker asthenosphere becomes decoupled from the lithosphere, it is more difficult to reconcile how the background strain rate could increase with depth.

Figure 6 shows a comparison of calculated time-series from the best-fitting hot and cold dislocation creep models to those observed. As with the diffusion models, these steady-state dislocation creep models fail to explain fast early displacement rates that give way to lower later rates. And as with the diffusion models, the hot geotherm model leads to a better fit to the 7-year cumulative displacements, whereas the cold geotherm model shows greater changes in displacement rates. No combinations of steady-state dislocation creep and environmental parameters can be found that leads to calculated surface displacements consistent with the rate changes observed. This leads us to conclude that steady-state dislocation creep of wet olivine cannot by itself explain post-Hector Mine displacement time-series.

For dislocation creep models of wet olivine with background strain rates of 0.1 μstrain/yr, background differential stress levels are of the order of 0.03–0.07 MPa at 50 km depth depending on the assumed geotherm. This is about the same magnitude as coseismic stress changes imparted to these depths by the Hector Mine earthquake. For our next set of models we set the background strain rate at a relatively low value of 0.01 μstrain/yr, an order of magnitude less than that observed at the surface. Such models have much lower mantle background differential stresses (order 0.01 MPa at 50 km depth), which are much less than coseismic stress changes. Such models allow us to explore how stress-dependence could lead to significant postseismic displacement rate changes.

A stress-dependent rheology will become weaker (lower viscosity) when the stress increases. For models with a small background differential stress, coseismic stress increases should act to dramatically decrease the viscosity of the mantle directly beneath the rupture zone. Viscosity levels will recover as coseismic stresses are relaxed. These large viscosity changes could dramatically alter the rate of flow and therefore the rate of surface displacements, potentially explaining the rapid change in surface displacement rates observed (e.g. Freed et al. 2006). In the previous dislocation creep models discussed above, where background strain rates were relatively high (0.15 μstrain/yr or greater), coseismic stress changes do not have this effect. This explains why these models could not match the observed displacement rate changes despite the stress-dependence of these rheologies.

A mantle background strain rate much lower than that at the surface is justifiable from shear-wave splitting studies of seismic anisotropy. Shear-wave splitting data from below the Mojave Desert show an E–W trending fabric perpendicular to the surface deformation trend (Polet and Kanamori, 2002), indicating that the mantle at depth might indeed be decoupled from the lithosphere above. Though the seismic data provides little resolution as to the depth distribution

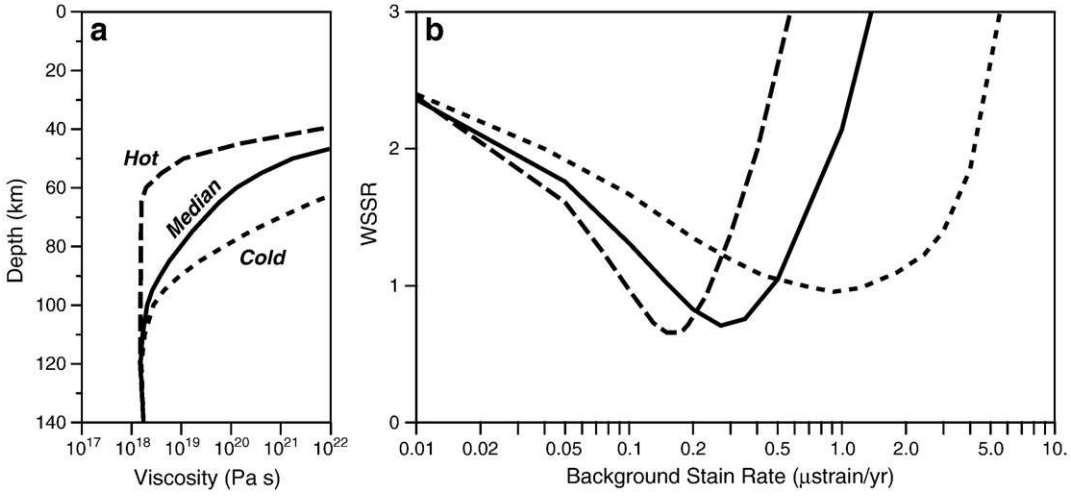

Fig. 5. (a) Calculated viscosity based on dislocation creep of wet olivine (median parameters, Table 1), a differential stress of 0.3 MPa, water content of 800 H/10^6Si, and the three thermal gradients shown in Figure 3a. (b) Misfit of calculated cumulative (7 years) postseismic surface displacements as a function of background strain rate and thermal gradient.

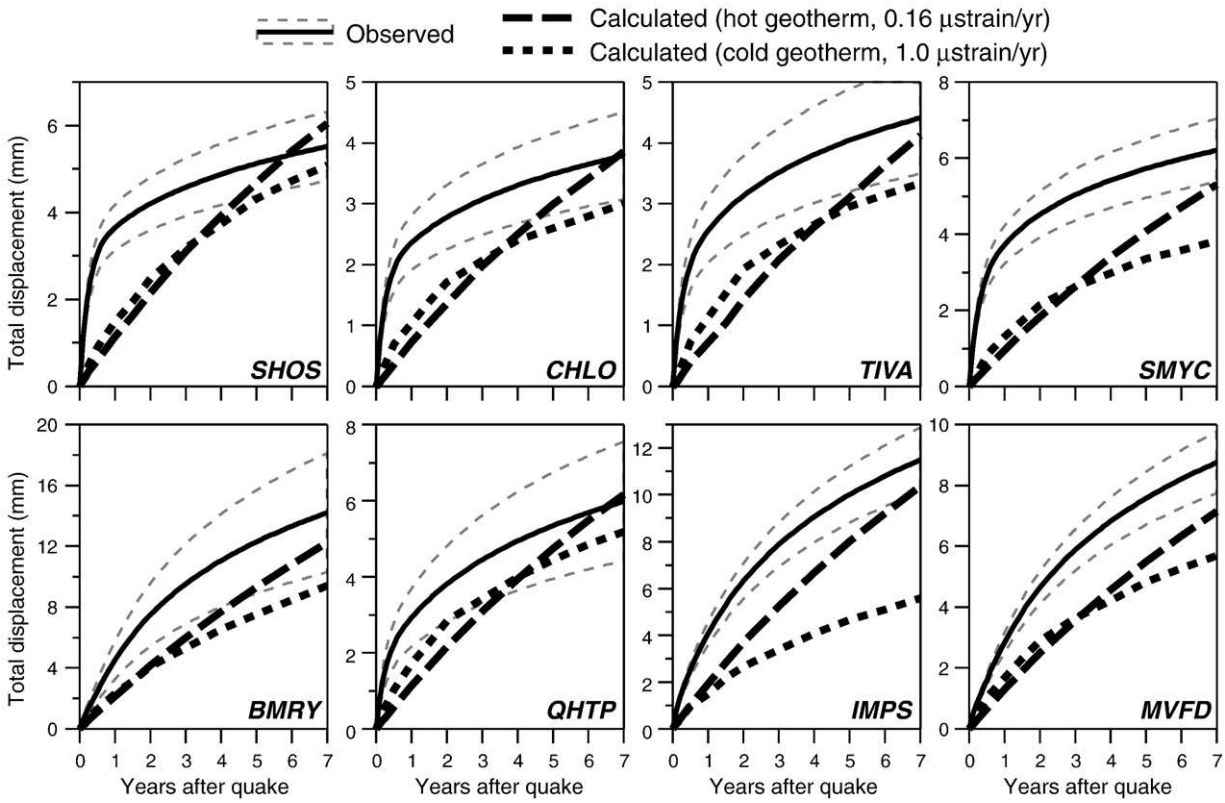

Fig. 6. Same as Figure 4, but for the two best-fitting dislocation creep models with varying thermal gradients and background strain rates.

of the anisotropic structure, Bonnin et al. (2010) argue that the E–W fabric is contained in an asthenospheric layer below a depth of 50 to 80 km. This would place it in the depth range at which the present analysis suggests decoupling.

In order to for a dislocation creep model with a low background strain rate to be weak enough for postseismic flow to be significant enough to explain observed 7 year cumulative surface displacements, the geotherm needs to be much hotter than those previously considered. This is because high temperatures, which decrease viscosity, are required to compensate for low background stresses, which lead to an increase in viscosity levels. Figure 7 shows the geotherm required to enable a model with a background strain rate of 0.01 μstrain/yr to explain 7-year cumulative surface displacements. It requires a sudden increase in the thermal gradient at 40 km depth and temperatures of 1700° at a depth of 50 km. This geotherm is not plausible, and thus the model is not realistic. Nevertheless, Figure 8 shows that a low background strain rate model can be used to reasonably match time-series displacements following the Hector Mine earthquake. Thus, stress-dependence has the capability to influence rate changes observed in postseismic displacements, though a plausible steady-state dislocation creep model could not be found given observational constraints on the thermal gradient beneath the Mojave Desert.

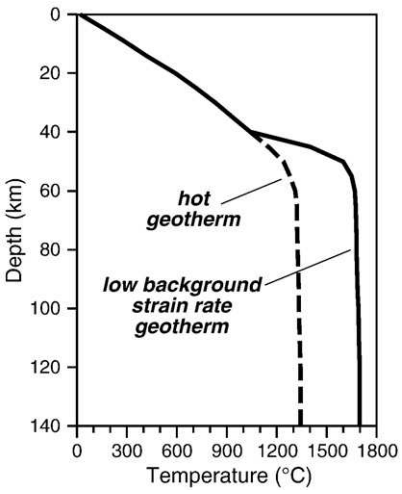

Fig. 7. Comparison of the seismically inferred hot geotherm and one required for a model that assumes a low background strain rate (0.01 μstrain/yr) to fit cumulative postseismic displacements.

5. Discussion

Steady-state diffusion or dislocation creep flow laws associated with wet olivine cannot be used to explain surface displacement time-series following the 1999 Hector Mine earthquake, though a dislocation model can be made to work using implausible tectonic conditions. The implication is that the response is non-steady-state, perhaps the transient response to sudden changes in loading conditions that has been observed in the laboratory (Carter and Kirby, 1978; Chopra, 1997). The existence of a transient weakening phase of mantle flow in response to an earthquake would provide a means to generate fast early surface displacements rates in such a manner that flow characteristics after this time period may very well be consistent with steady-state flow law parameters for olivine as currently reported in the laboratory.

Though transient behavior has been shown to work well to explain initial postseismic displacement rates (Hearn et al., 2009; Pollitz, 2003, 2005), such studies have to date not considered the temperature- and stress-dependence of this phase (Chopra, 1997). Instead such analyses have simply solved for the average viscosity of the transient and steady-state phases (Burgers body) that lead to the best fit to observed postseismic constraints. Such an approach is valid only to describe a specific response to a specific earthquake within a

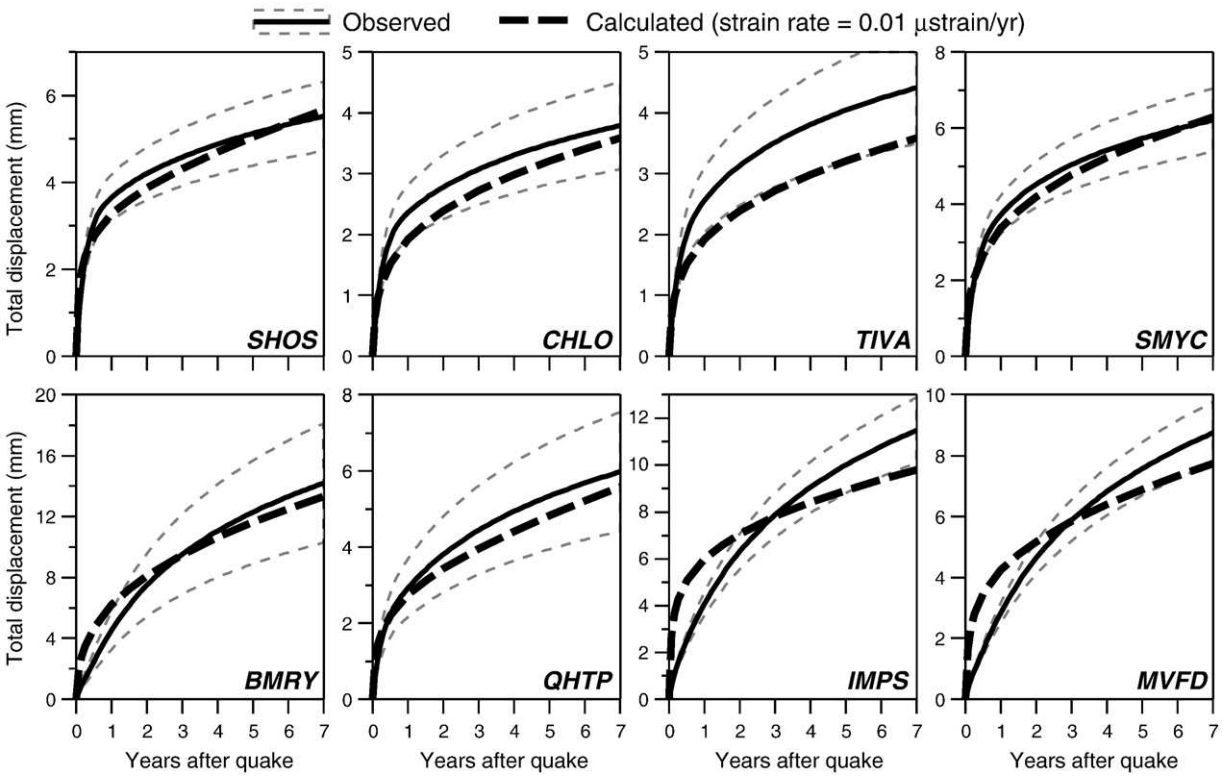

Fig. 8. Same as Figure 4, but for a model that assumes a low background strain rate of 0.01 μstrain/yr and the low background strain rate geotherm shown in Figure 7.

specific tectonic environment. It does not provide a means to understand how transient and steady-state viscosity structure is influenced by environmental parameters. If postseismic observations of transient and steady-state behavior can be described by a constitutive relationship that incorporates flow law and environmental parameters, this would enable an understanding and prediction of the response of the crust and mantle to any change in stress associated with any tectonic environment. It would also allow for a more direct test of laboratory derived flow law parameters.

Controls on the viscosity of olivine in the transient phase are only beginning to be constrained by laboratory experiments. Chopra (1997) reports that the ratio of the effective viscosities of the transient to steady-state regimes (between 0.17 and 0.67) appears to be insensitive to temperature and stress. Though this is a fairly broad range, it is well above the ratios inferred from most postseismic studies that consider transient rheology: 0.035 (Pollitz, 2003), 0.036 (Pollitz, 2005), 0.05 (Pollitz et al., 2008), and 0.1–0.25 (Hearn et al., 2009). This difference may be associated with the difficulty of extracting effective viscosities from postseismic observations due to the influence of other postseismic mechanisms or limited spatial and temporal extents of the observations in previous studies. This discrepancy may also be due to the aforementioned neglected stress-dependence of the transient weakening phase. As the transient phase appears to share the same dependence of stress as the steady-state phase (Chopra, 1997), the change in viscosity with time associated with such power-law dependence could significantly influence a postseismic analysis.

6. Conclusions

Postseismic displacements at far-field GPS stations following the 1999 Hector Mine earthquake have previously been identified as resulting from flow due to viscoelastic relaxation within the upper mantle (Freed et al., 2007). Here we tested whether laboratory derived steady-state flow laws for wet olivine could be used to explain observed displacement time-series rate changes at these far-field stations. We found that steady-state flow laws associated with neither diffusion nor dislocation creep of wet olivine could be used to explain the observed time-series, though a dislocation creep model can be made to work using implausibly hot conditions.

We conclude that a non-steady-state viscoelastic response is being observed initially following the Hector Mine earthquake, probably a transient weakening mechanism in response to changing loading conditions. While an initial transient weakening process has been previously suggested to explain observed postseismic time-series, such analyses assumed linear rheologies and have overestimated the degree to which viscosities are decreased in the transient phase compared to steady-state flow according to laboratory experiments. This discrepancy may be due to the lack of consideration of stress-dependence in postseismic transient rheology studies to date.

Having established that a transient phase is likely present and prominent in postseismic relaxation processes, experimentalists will hopefully be motivated to further investigate the nature of transient behavior in a broad range of tectonic environments, and postseismic analyses should begin to consider incorporating temperature- and stress-dependent laboratory flow laws of transient and steady-state behavior. These dual lines of research will help the development of a general constitutive relationship that can explain the response of the upper mantle to any tectonic environment over any time period.

Acknowledgements

We thank two anonymous reviewers for the suggested changes that greatly improved the manuscript. We thank Jun Korenaga for help in understanding covariances between flow law parameters and their influence on uncertainties in viscosity. This research was funded by NSF Earthscope grant EAR-0952234.

Appendix A. Supplementary data

Supplementary data to this article can be found online at doi:10.1016/j.epsl.2010.10.005.

References

Altamini, Z., Collilieux, X., Legrand, J., Garayt, B., Boucher, C., 2007. ITRF2005: a new release of the International Terrestrial Reference Frame based on time series of station positions and Earth Orientation Parameters. J. Geophys. Res. 112, B09401. doi:10.1029/2007JB004949.

Bell, D.R., Rossman, G.R., 1992. Water in Earth's mantle — the role of nominally anhydrous minerals. Science 255, 1391–1397.

Bonnin, M., Barruol, G., Bokelmann, G.H.R., 2010. Upper mantle deformation beneath the North American–Pacific plate boundary in California from SKS splitting. J. Geophys. Res. 115, B04306. doi:10.1029/2009JB006438.

Borch, R.S., Green II, H.W., 1987. Dependence of creep in olivine on the homologous temperature and its implications for flow in the mantle. Nature 330, 345–348.

Bürgmann, R., Dresen, G., 2008. Rheology of the lower crust and upper mantle: evidence from rock mechanics, geodesy and field observations. Ann. Rev. Earth Planet. Sci. 36, 531–567.

Carter, N.L., Kirby, S., 1978. Transient creep and semi-brittle behavior of crystalline rocks. Pure Appl. Geophys. 116, 807–839.

Carter, N.L., Tsenn, M.C., 1987. Flow properties of continental lithosphere. Tectonophys 136, 27–63.

Chopra, P.N., 1997. High-temperature transient creep in olivine rocks. Tectonophys 279, 93–111.

Ferland, R., 2006. From relative to absolute phase center calibrations: the effects on the SINEX products, paper ABS4. Proceedings of the IGS Darmstadt Workshop, Darmstadt. Available at http://nng.esoc.esa.de/ws2006/Papers/10_Ferland_Phase.pdf.gz. Specific implementation available as: ftp://igscb.jpl.nasa.gov/igscb/station/coord/IGS05.SNX.Z. See also http://igscb.jpl.nasa.gov/overview/pubs/06_darmstadt.html.

Fialko, Y., 2004. Probing the mechanical properties of seismically active crust with space geodesy: study of the coseismic deformation due to the 1992 M w 7.3 Landers (southern California) earthquake. J. Geophys. Res. 109, B03307. doi:10.1029/2003JB002756.

Freed, A.M., Bürgmann, R., 2004. Evidence of power-law flow in the Mojave Desert mantle. Nature 430, 548–551.

Freed, A.M., Bürgmann, R., Calais, E., Freymueller, J., 2006. Stress-dependent power-law flow in the upper mantle following the 2002 Denali, Alaska, earthquake. Earth Planet. Sci. Lett. 252, 481–489.

Freed, A.M., Bürgmann, R., Herring, T., 2007. Far-reaching transient motions after Mojave earthquakes require broad mantle flow beneath a strong crust. Geophys. Res. Lett. 34. doi:10.1029/2007GL030959.

Handy, M.R., 1990. The solid-state flow of polymineralic rocks. J. Geophys. Res. 95, 8647–8661.

Hearn, E.H., McClusky, S., Ergintav, S., Reilinger, R.E., 2009. Izmit earthquake postseismic deformation and dynamics of the North Anatolian Fault Zone. J. Geophys. Res. 114, B08405. doi:10.1029/2008JB006026.

Hirth, G., Kohlstedt, D.L., 1995. Experimental constraints on the dynamics of the partially molten upper mantle: deformation in the diffusion creep regime. J. Geophys. Res. 100, 1981–2001.

Hirth, G., Kohlstedt, D.L., 1996. Water in the oceanic mantle: Implications for rheology, melt extraction, and the evolution of the lithosphere. Earth Planet. Sci. Lett. 144, 93–108.

Hirth, G., Teyssier, C., Dunlap, W.J., 2001. An evaluation of quartzite flow laws based on comparisons between experimentally and naturally deformed rocks. Int. J. Earth Sci. 90, 77–87.

Hirth, G., Kohlstedt, D.L., 2003. Rheology of the upper mantle and the mantle wedge: a view from the experimentalists. In: Eiler, J. (Ed.), The subduction factory: Geophys. Monogr. Ser., 138, pp. 83–102.

Hyndman, R.D., Currie, C.A., Mazzotti, S., Frederiksen, A., 2009. Temperature control of continental lithosphere elastic thickness, Te vs Vs. Earth Planet. Sci. Lett. 277, 539–548. doi:10.1016/j.epsl.2008.11.023.

Jung, H., Katayama, I., Jiang, Z., Hiraga, T., Karato, S., 2006. Effect of water and stress on the lattice-preferred orientation of olivine. Tectonophysics 421, 1–22.

Karato, S.-I., 1997. Phase transformations and rheological properties of mantle minerals. In: Croosley, D. (Ed.), Earth's Deep Interior. Gordon and Breach, NJ, pp. 223–272.

Karato, S., 1986. Does partial melting reduce the creep strength of the upper mantle? Nature 319, 309–310.

Karato, S., Wu, P., 1993. Rheology of the upper mantle: a synthesis. Science 260, 771–778.

Kirby, S.H., Kronenberg, A.K., 1987. Rheology of the lithosphere; selected topics. Rev. Geophys. 25, 1219–1244.

Korenaga, J., Karato, S.-I., 2008. A new analysis of experimental data on olivine rheology. J. Geophys. Res. 113, B02403. doi:10.1029/2007JB005100.

Mei, S., Kohlstedt, D.L., 2000a. Influence of water on plastic deformation of olivine aggregates, 1. Diffusion creep regime. J. Geophys. Res. 105 (21) 457–21,469.

Mei, S., Kohlstedt, D.L., 2000b. Influence of water on plastic deformation of olivine aggregates, 2. Dislocation creep regime. J. Geophys. Res. 105 (21) 471–21,481.

Pollitz, F.F., 2003. Transient rheology of the uppermost mantle beneath the Mojave Desert, California. Earth Planet. Sci. Lett. 215, 89–104.

Polet, J., Kanamori, H., 2002. Anisotropy beneath California: shear wave splitting measurements using a dense broadband array. Geophys. J. Int. 149, 313–327.

Pollitz, F.F., 2005. Transient rheology of the upper mantle beneath central Alaska inferred from the crustal velocity field following the 2002 Denali earthquake. J. Geophys. Res. 110. doi:10.1029/2005JB003672.

Pollitz, F.F., Banerjee, P., Grijalva, K., Nagarajan, B., Bürgmann, R., 2008. Effect of 3-D viscoelastic structure on post-seismic relaxation for the 2004 M = 9.2 Sumatra earthquake. Geophys. J. Int. 173 (1), 189–204. doi:10.111/j.1364/246X2007.03666.x.

Savage, J.C., Svarc, J.L., Prescott, 2003. Near-field postseismic deformation associated with the 1992 Landers and 1999 Hector Mine, California, earthquakes. J. Geophys. Res. 108. doi:10.1029/2002JB002330.

Simons, M., Fialko, Y., Rivera, L., 2002. Coseismic deformation from the 1999 Mw 7.1 Hector Mine, California, Earthquake as inferred from InSAR and GPS observations. Bull. Seismol. Soc. Am. 92, 1390–1402.

Yang, Y., Forsyth, D.W., 2008. Attenuation in the upper mantle beneath Southern California: physical state of the lithosphere and asthenosphere. J. Geophys. Res. 113. doi:10.1029/2007JB005118.